The SIRT1 deacetylase protects mice against the symptoms of metabolic syndrome

Annabelle Z. Caron,* Xiaohong He,* Walid Mottawea,† Erin L. Seifert,‡ Karen Jardine,* Danielle Dewar-Darch,* Greg O. Cron,* Mary-Ellen Harper,† Alain Stintzi,† and Michael W. McBurney*,†,1

*Ottawa Hospital Research Institute and †Department of Biochemistry, Microbiology, and Immunology, University of Ottawa, Ottawa, Ontario, Canada; and ‡Thomas Jefferson University, Philadelphia, Pennsylvania, USA

ABSTRACT **Type 2 diabetes, hepatic steatosis, and gut dysbiosis are pathophysiological consequences of obesity. Sirtuin (SIRT)-1 is a protein deacetylase implicated in the regulation of metabolic activity. We set out to determine whether the catalytic activity of SIRT1 plays a role in the development of metabolic syndrome, hepatic steatosis, and the distribution of gut microbiota. We challenged with a high-fat diet (HFD) a strain of mice homozygous for a *Sirt1* allele carrying a point mutation that ablates the deacetylase activity of SIRT1. When compared to wild-type animals, mice lacking SIRT1 catalytic activity rapidly accumulated excessive hepatic lipid while fed the HFD, an effect evident within 2 wk of HFD feeding. Both white and brown adipose depots became hypertrophic, and the animals developed insulin resistance. The ratio of the major phyla of gut microbiota (Firmicutes and Bacteroidetes) increased rapidly in the SIRT1-deficient mice after HFD challenge. We conclude that the deacetylase activity of SIRT1 plays an important role in regulating glucose and hepatic lipid homeostasis. In addition, the composition of gut microbiota is influenced by both the animals' *Sirt1* genotype and diet composition.—Caron, A. Z., He, X., Mottawea, W., Seifert, E. L., Jardine, K., Dewar-Darch, D., Cron, G. O., Harper, M.-E., Stintzi, A., McBurney, M. W. The SIRT1 deacetylase protects mice against the symptoms of metabolic syndrome. *FASEB J.* 28, 1306–1316 (2014). www.fasebj.org**

Key Words: fatty liver · gut microbiota · high-fat diet

Metabolic syndrome is a combination of metabolic abnormalities associated with obesity, hyperglycemia, insulin resistance, fatty liver, and systemic inflammation. It is an increasingly important health concern in Western society because it predisposes to type 2 diabetes and cardiovascular disease. In humans, etiology is complex, but in experimental rodents, the condition can be readily induced by feeding animals diets with high calorie content, such as a high-fat diet (HFD).

A growing body of evidence indicates that the composition of gut microbiota contributes to the pathology of obesity and metabolic syndrome. Obese mice have an altered gut microbiome compared with that of lean individuals (1), and the genetic predisposition to obesity influences the composition of the gut microbiome (2). The sirtuins (SIRTs) are cellular proteins that may contribute to the modulation of gut microbe composition.

The SIRT family of proteins is characterized by the presence of a catalytic domain that couples NAD^+ hydrolysis to protein deacetylation (3–5). SIRT1 is the most studied of the mammalian SIRTs and is a nuclear protein expressed in all tissues, albeit at variable levels (6). The spectrum of acetylated protein substrates of SIRT1 is vast, with >80 now documented (7). Among the SIRT1 substrates are several proteins that regulate metabolic activity, mitochondrial biogenesis, fatty acid metabolism, and glucose homeostasis (8, 9). These include forkhead box class O (FOXO) proteins (10), peroxisome proliferator activated receptor γ coactivator 1α (PGC-1α; refs. 9, 11, 12), peroxisome proliferator activated receptor γ (PPARγ; ref. 8), liver X receptor (LXR; ref. 13), and farsenoid X receptor (FXR; ref. 14). Modulating the activities of these substrates is thought to allow the organism, particularly the liver, to acclimate to a diet enriched in fatty acids and abundant energy sources.

Consistent with a role for SIRT1 in regulating metabolic functions is that mice lacking it have elevated rates of respiration (15), a characteristic that most likely causes the *Sirt1*-null mice to be smaller than their

Abbreviations: BAT, brown adipose tissue; FXR, farsenoid X receptor; H&E, hematoxylin and eosin; HFD, high-fat diet; LXR, liver X receptor; OGTT, oral glucose tolerance test; OTU, operational taxonomic unit; PGC-1α, peroxisome proliferator activated receptor γ coactivator 1α; PPARγ, peroxisome proliferator activated receptor γ; RER, respiratory exchange ratio; SIRT, sirtuin; UCP1, uncoupling protein 1; $V\text{co}_2$, carbon dioxide production rate; $V\text{o}_2$, oxygen consumption rate; WAT, white adipose tissue

[1] Correspondence: Program in Cancer Therapeutics, Department of Medicine, Ottawa Hospital Research Institute, University of Ottawa, Box 926, 501 Smyth Road, Ottawa, ON, Canada K1H 8L6. E-mail: mmcburney@ohri.ca

doi: 10.1096/fj.13-243568

0892-6638/14/0028-1306 © FASEB

normal littermates and to accumulate less white adipose tissue (WAT; ref. 16). We recently engineered a strain of mice harboring a point mutation within the catalytic domain of the *Sirt1* gene. This mutant allele (*Sirt1*$^{tm2.1Mcby}$, abbreviated here as *Sirt1*^{Y}) encodes a protein, SIRT1(H335Y), that has undetectable catalytic activity (17). Homozygous *Sirt1*$^{Y/Y}$ mice, like *Sirt1*$^{-/-}$ mice, have elevated levels of respiration, smaller stature, and reduced depots of WAT.

We set out to determine whether *Sirt1*$^{Y/Y}$ mice respond aberrantly to diets rich in fat. Despite their elevated rates of respiration, we report that these animals developed more severe characteristics of metabolic syndrome than did their wild-type littermates, indicating that the catalytic activity of SIRT1 plays an important role in the acclimation of mice to diets rich in calories, perhaps by influencing the composition of the gut microbiome.

MATERIALS AND METHODS

Animal experiments

The mice used in this study carried a point mutation in the *Sirt1* gene, *Sirt1*$^{tm2.1Mcby}$ (*Sirt1*^{Y}), that encodes the protein SIRT1(H355Y), with no detectible catalytic activity (17). The *Sirt1*^{Y} allele was maintained on a mixed genetic background derived from intercrosses between the CD1 and 129/svJ mice. The *Sirt1* genotypes of animals were determined by a PCR-based test performed on DNA isolated from tail-tip biopsies by using the primers 5′-TGGAAGGAAAGCAATTTTGGT-3′ and 5′-CTGAGTTACCTTAGCTTGGC-3′. *Sirt1*$^{Y/Y}$ males and their *Sirt1*$^{+/+}$ littermates were caged individually with woodchip bedding. Mice 2–3 mo of age were divided into 2 dietary groups: standard chow (18% protein rodent diet; Harlan Laboratories, Madison, WI, USA) or an HFD (60% of calories from fat; Bioserv, Frenchland, NJ, USA). The food intake and body weight of each mouse in all groups was recorded weekly. All animals were euthanized in the morning (09:00 to 12:00). Animal experimentation was conducted in accordance with the guidelines of the Canadian Council for Animal Care, with protocols approved by the Animal Care Committee of the University of Ottawa.

Blood glucose, insulin, and leptin

Mice were euthanized in the morning after 18 h of food withdrawal. Blood samples were obtained by intracardiac puncture immediately after terminal CO_2 inhalation. The blood was centrifuged (15,000 *g*, 15 min at 4°C), and the serum was stored at −80°C until analysis. Insulin was measured with the ultrasensitive mouse insulin ELISA kit (Crystal Chem, Downers Grove, IL, USA). Leptin was measured with the rat and mouse leptin ELISA kit (Innovative Research, Southfield, MI, USA). For the glucose tolerance test, the mice were unfed overnight and gavaged with glucose solution (2 g/kg body weight). Blood glucose levels were measured with OneTouch Ultra glucose meter and strips (LifeScan Canada, Burnaby, BC, Canada), before and at 15, 30, 45, 60, 90, 120, and 150 min after gavage.

Indirect calorimetry and activity

Indirect calorimetry was performed with a 4-chamber, open-circuit, indirect calorimeter (Oxymax; Columbus Instruments, Columbus, OH, USA). Mice were placed in individual cages supplied with air at 0.5 L/min and maintained at 24°C with lights on from 06:00 to 18:00. In each chamber, the concentrations of O_2 and CO_2 were measured, and the data were collected over 24 h periods. The respiratory exchange ratio (RER) was calculated as the ratio of oxygen consumption ($V\!o_2$) to carbon dioxide production ($V\!co_2$). $V\!o_2$ values were normalized to body weight. Ambulatory activity of each animal was measured simultaneously with the optical beam technique (Opto M_3; Columbus Instruments). Consecutive photobeam breaks were scored as a horizontal ambulatory movement. Activity counts were recorded every minute for 24 h. Measurements were taken before the HFD started and after 4 and 12 wk of the HFD.

The effect of the β_3-selective adrenergic agonist CL-316243 on metabolic rate was measured as follows, with each mouse serving as its own control. At 09:00, mice were placed into the calorimetry chamber, and baseline data were collected. After 3 h, CL-316243 was injected intraperitoneally (1 mg/kg body weight), and after a 1 h delay, data were collected for 3 h.

Electrophoresis and immunoblot analysis

Liver tissues were homogenized in ice-cold RIPA buffer (0.5% Nonidet P-40, 0.1% sodium deoxycholate, 150 mM NaCl, and 50 mM Tris-HCl, pH 7.5) supplemented with Complete protease inhibitor cocktail (Roche Molecular Biochemicals, Laval, QC, Canada) in a borosilicate glass Dounce tissue grinder (1 ml) with tight pestle (Wheaton Industries, Schaumburg, IL, USA). The homogenates were centrifuged at 15,000 rpm for 10 min at 4°C, and the supernatants were collected. Protein extracts (30 μg) were separated on a NuPAGE Bis-Tris 4–12% gradient precast polyacrylamide gel (Invitrogen, Burlington, ON, Canada), electrotransferred to a nitrocellulose membrane. Blotted membranes were incubated overnight at 4°C with anti-SIRT1 (1:500; cat. no. 2028) and anti-α-tubulin (1:1000; 2125), both from Cell Signaling Technology (Danvers, MA, USA). Anti-UCP1 (1:1000; Sc-6529) was from Santa Cruz Biotechnology (Santa Cruz, CA, USA), and anti-actin (1:10,000; A5316) was from Sigma-Aldrich (St. Louis, MO, USA). Bands were visualized with Luminata Forte Western HRP substrate (Millipore, Billerica, MA, USA), according to the manufacturer's instructions, on BioMax ML film (Kodak, Rochester NY, USA). Signals were quantitated by densitometry with ImageJ software (U.S. National Institutes of Health, Bethesda, MD, USA).

Histology

Formalin-fixed, paraffin-embedded livers [WAT and brown adipose tissue (BAT)] were cut into 5-μm sections and stained with hematoxylin and eosin (H&E). The frozen livers embedded in optimal cutting temperature (OCT) compound (Tissue-Tek; Sakura Finetek, Torrance, CA, USA) were sectioned at 6 μm and stained with Oil Red O (American Master Tech, Lodi, CA, USA), according to a standard protocol. Briefly, the liver cryosections were fixed for 10 min in 10% formalin and rinsed 3 times with ddH_2O. The samples were dehydrated for 5 min in 100% propylene glycol, stained with 0.5% Oil Red O in propylene glycol for 10 min at 60°C, rinsed in 85% propylene glycol, and extensively washed with ddH_2O. For nuclear staining, samples were incubated for 30 s in hematoxylin solution and rinsed in ddH_2O. After a final rinsing in ddH_2O, the sections were mounted with aqueous mounting medium (Mandel Scientific, Guelph, ON, Canada). Staining was digitized with the Aperio ScanScope and analyzed with Aperio ImageScope software (Axiovision Technologies, Toronto, ON, Canada).

TABLE 1. *Primers used in constructing the Illumina library*

rDNA	Primer
MF1	5′-ACACTCTTTCCCTACACGACGCTCTTCCGATCTATAGCGAAACTCAAAKGAATTGACGG-3′
MF2	5′-ACACTCTTTCCCTACACGACGCTCTTCCGATCTAGGGTAAACTCAAAKGAATTGACGG-3′
MF3	5′-ACACTCTTTCCCTACACGACGCTCTTCCGATCTTTCATAAACTCAAAKGAATTGACGG-3′
MF4	5′-ACACTCTTTCCCTACACGACGCTCTTCCGATCTGATCGTAAACTCAAAKGAATTGACGG-3′
MF5	5′-ACACTCTTTCCCTACACGACGCTCTTCCGATCTGCCCGTAAACTCAAAKGAATTGACGG-3′
MF6	5′-ACACTCTTTCCCTACACGACGCTCTTCCGATCTCTGTCAAACTCAAAKGAATTGACGG-3′
MF7	5′-ACACTCTTTCCCTACACGACGCTCTTCCGATCTCACGTAAACTCAAAKGAATTGACGG-3′
MF8	5′-ACACTCTTTCCCTACACGACGCTCTTCCGATCTCGTACGAAACTCAAAKGAATTGACGG-3′
MF9	5′-ACACTCTTTCCCTACACGACGCTCTTCCGATCTGGACAAACTCAAAKGAATTGACGG-3′
MF10	5′-ACACTCTTTCCCTACACGACGCTCTTCCGATCTTAGAAAACTCAAAKGAATTGACGG-3′
MF11	5′-ACACTCTTTCCCTACACGACGCTCTTCCGATCTTCATAAACTCAAAKGAATTGACGG-3′
MF12	5′-ACACTCTTTCCCTACACGACGCTCTTCCGATCTACTTAAACTCAAAKGAATTGACGG-3′
MR1	5′-CTCGGCATTCCTGCTGAACCGCTCTTCCGATCTATAGCGAACGAGCTGACGACARCCATG-3′
MR2	5′-CTCGGCATTCCTGCTGAACCGCTCTTCCGATCTAGGGTAACGAGCTGACGACARCCATG-3′
MR3	5′-CTCGGCATTCCTGCTGAACCGCTCTTCCGATCTTTCATAACGAGCTGACGACARCCATG-3′
MR4	5′-CTCGGCATTCCTGCTGAACCGCTCTTCCGATCTGATCGTAACGAGCTGACGACARCCATG-3′
MR5	5′-CTCGGCATTCCTGCTGAACCGCTCTTCCGATCTGCCCGTAACGAGCTGACGACARCCATG-3′
MR6	5′-CTCGGCATTCCTGCTGAACCGCTCTTCCGATCTCTGTCAACGAGCTGACGACARCCATG-3′
MR7	5′-CTCGGCATTCCTGCTGAACCGCTCTTCCGATCTCACGTAACGAGCTGACGACARCCATG-3′
MR8	5′-CTCGGCATTCCTGCTGAACCGCTCTTCCGATCTCGTACGAACGAGCTGACGACARCCATG-3′
MR9	5′-CTCGGCATTCCTGCTGAACCGCTCTTCCGATCTGGACAACGAGCTGACGACARCCATG-3′
MR10	5′-CTCGGCATTCCTGCTGAACCGCTCTTCCGATCTTAGAAACGAGCTGACGACARCCATG-3′
MR11	5′-CTCGGCATTCCTGCTGAACCGCTCTTCCGATCTTCATACGAGCTGACGACARCCATG-3′
MR12	5′-CTCGGCATTCCTGCTGAACCGCTCTTCCGATCTACTTACGAGCTGACGACARCCATG-3′
PCRFWD1	5′-AATGATACGGCGACCACCGAGATCTACACTCTTTCCCTACACGACGCTCTTCCGATCT-3′
PCRRVS1	5′-CAAGCAGAAGACGGCATACGAGATCGGTCTCGGCATTCCGTCTGAACCGCTCTTCCGATCT-3′

Underscored nucleotides represent the barcode sequences.

Triglyceride measurement in the liver

Analysis of hepatic triglyceride content was performed by ethanolic potassium hydroxide (KOH) saponification, followed by an assay for glycerol (18). Briefly, liver tissue (0.3 g) was subjected to saponification in ethanol-KOH (2 parts ethanol:1 part 30% KOH) at 55°C. After overnight incubation, the volume of the digested tissue was adjusted to 1 ml with 50% ethanol and centrifuged for 5 min at 10,000 *g*. The supernatant was diluted to 1.2 ml with 50% ethanol and vortexed. A volume of 200 μl of the supernatant was mixed to 215 μl of $MgCl_2$ (1 M), vortexed, and incubated on ice for 10 min. The material was centrifuged for 5 min at 10,000 *g*, and the supernatant was analyzed for glycerol content with free glycerol reagent (F6428; Sigma-Aldrich), and the concentration was determined by using a standard glycerol solution (G7793; Sigma-Aldrich).

MRI acquisition

MRI was performed with a Discovery MR 901 7-T small animal scanner (GE/Agilent, Santa Clara, CA, USA), equipped with a 72-mm (inner diameter) transmit-and-receive coil. The pulse sequence used was a 3D fast gradient-recalled echo with the following parameters: repetition time, 12 ms; echo time, 2 ms; flip angle, 60°; bandwidth, 250 kHz; field of view, 10 × 5 cm; matrix, 512 × 256 × 64; spatial resolution, 0.2 × 0.2 × 0.4 mm; and 2 averages, scan time, 3 min.

Immunohistochemistry

Formalin-fixed, paraffin-embedded livers were cut into 5-μm sections, deparaffinized, and rehydrated. The sections were blocked for nonspecific binding with Protein Block, serum-free solution (Dako, Glostrup, Denmark) and incubated with the primary antibody anti-SIRT1 (1:50; 2028; Cell Signaling Technology) in a humidified chamber at room temperature overnight. The sections were then incubated with an HRP-labeled polymer conjugated with rabbit secondary antibody (Dako) for 30 min at room temperature. A dark brown

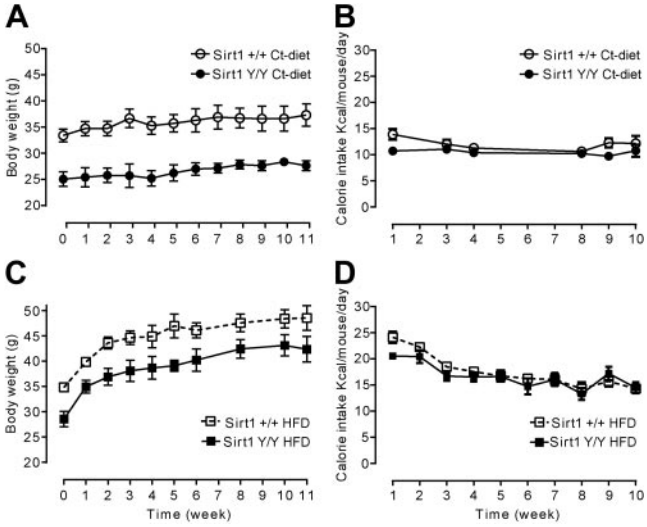

Figure 1. *Sirt1*$^{Y/Y}$ mice are small and hyperphagic. Male *Sirt1*$^{+/+}$ and *Sirt1*$^{Y/Y}$ mice, 2–3 mo of age, were fed either the normal chow control diet (*A*, *B*) or an HFD (*C*, *D*). Weights of each animal were recorded weekly (*A*, *C*) along with daily calorie intake (*B*, *D*). Data are means ± SE from groups of 3 *Sirt1*$^{+/+}$ and 3 *Sirt1*$^{Y/Y}$ animals fed the control diet (*A*, *B*) and 9 *Sirt1*$^{+/+}$ and 10 *Sirt1*$^{Y/Y}$ mice fed the HFD (*C*, *D*).

substrate was developed with a freshly prepared chromogen/substrate DAB reagent solution (Sigma-Aldrich). The sections were mounted with Fluoromount (BDH Laboratories, Poole, UK). Staining was digitized with the Aperio ScanScope and analyzed with Aperio ImageScope software (Axiovision Technologies).

Microbiome analysis by 16S rDNA V6 sequencing

Metagenomic DNA was extracted from 100–200 mg of mouse stool with a Fast DNA Spin Kit (MP Biomedicals, Solon, OH, USA), according to the manufacturer's instructions. The 16S rDNA V6 library for Illumina (San Diego, CA, USA) sequencing was constructed from the extracted DNA according to the approach described by Arthur *et al.* (19). Briefly, the V6 region of 16S rDNA was amplified by 2 successive PCR reactions, to introduce the Illumina paired-end sequencing adapters, barcode sequences, and flow cell adapters; universal 16S rDNA-V6 primers modified from Sundquist *et al.* (20) were used (**Table 1**). PCR amplicons were quantified and pooled at an equimolar concentration. The library was sequenced at the Center for Applied Genomics (TCAG; SickKids, Toronto, ON, Canada) with 1 lane of a HiSeq 2500 (Illumina) used to generate paired-end reads of 2 × 101 bases. Obtained paired-end sequences were merged into longer reads with Fast Length Adjustment of Short Reads (FLASh) software (Johns Hopkins University, Baltimore, MD, USA), avoiding any mismatch in the overlap region, which ranges from 10 to 80 nt (21), and using the fastq file as input. More than 95% of the reads were merged successfully, whereas the sequences that failed to merge were discarded. The reads were quality filtered with a minimum quality score per base of 20 with the fastq_quality_filter command from the Fastx toolkit (Cold Spring Harbor Laboratory, Cold Spring Harbor, NY, USA; http://hannonlab.cshl.edu/). Next, the reads were binned into their original samples according to their 5′ and 3′ barcodes, and the barcodes were trimmed by using Novobarcode commands (Novocraft, Selangor, Malaysia; http://www.novocraft.com). High-quality sequences were clustered into operational taxonomic units (OTUs) *via* the closed-reference, OTU-picking workflow of Quantitative Insights Into Microbial Ecology (QIIME) 1.5.0 pipeline (http://qiime.wordpress.com; ref. 22), by using UCLUST against a Greengenes reference set (release 4, February 2011; http://greengenes.secondgenome.com/), based on an average percentage of identity of 97%. Singletons and doubletons were removed, and the resulting OTU table was used to summarize the taxonomy and to assess the α and β diversity within and among the samples, according to the default criteria of QIIME. A Mann-Whitney 2-tailed test was applied for pairwise comparison of the relative abundance of different taxa.

RESULTS

Hypertrophy of adipose tissues in *Sirt1*$^{Y/Y}$ mice fed an HFD

The *Sirt1*$^{Y/Y}$ animals were 20–30% smaller than their *Sirt1*$^{+/+}$ littermates when fed normal chow (**Fig. 1*A***), although the calorie intake of both strains was equal (Fig. 1*B*). When the *Sirt1*$^{Y/Y}$ mice were challenged with an HFD, their body weight increased in parallel with that of the *Sirt1*$^{+/+}$ animals (Fig. 1*C*), but the *Sirt1*$^{Y/Y}$

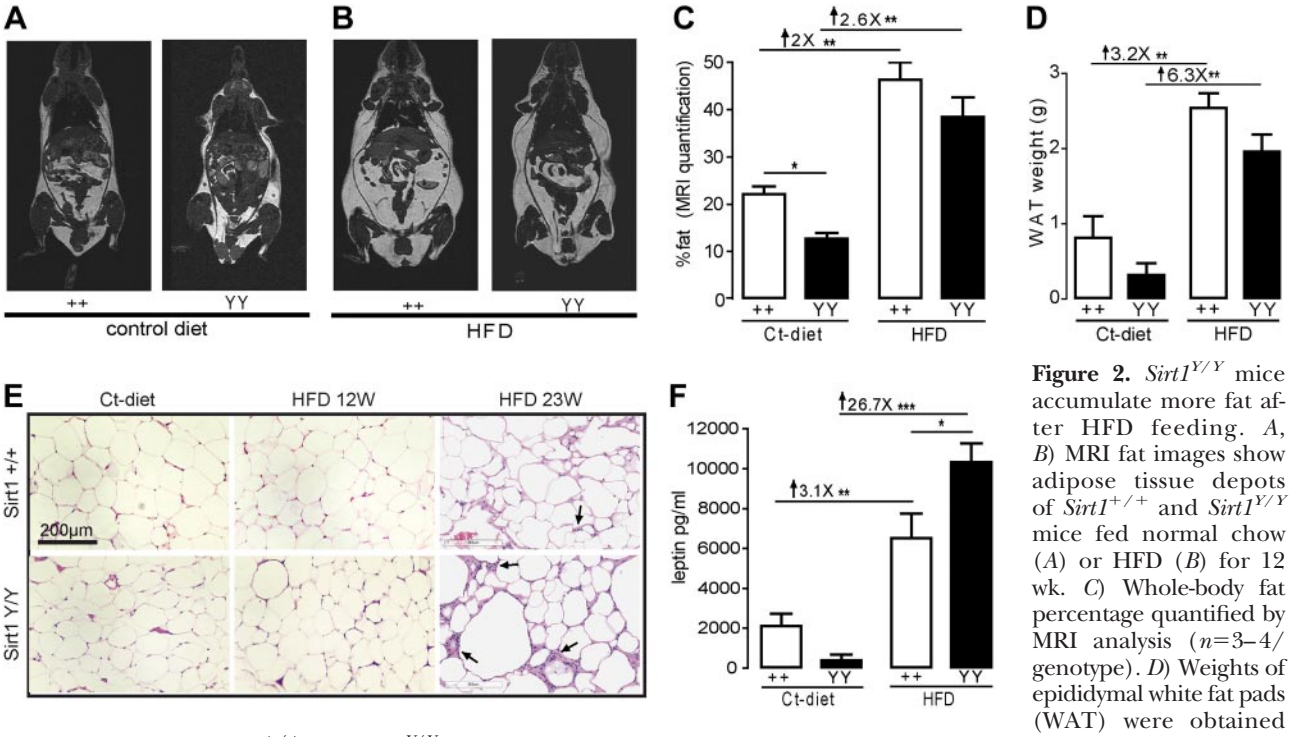

Figure 2. *Sirt1*$^{Y/Y}$ mice accumulate more fat after HFD feeding. *A*, *B*) MRI fat images show adipose tissue depots of *Sirt1*$^{+/+}$ and *Sirt1*$^{Y/Y}$ mice fed normal chow (*A*) or HFD (*B*) for 12 wk. *C*) Whole-body fat percentage quantified by MRI analysis (n=3–4/genotype). *D*) Weights of epididymal white fat pads (WAT) were obtained from 5- to 6-mo-old *Sirt1*$^{+/+}$ and *Sirt1*$^{Y/Y}$ mice fed a normal chow diet (n=3/genotype) or an HFD for 12 wk (n=9–10/genotype). *E*) Histologic sections from the WAT show enlarged unilocular vacuoles in both genotypes after HFD feeding and infiltration of lymphoid cells (arrows) after 23 wk of HFD that were particularly abundant in WAT from *Sirt1*$^{Y/Y}$ mice. *F*) Leptin levels in blood of *Sirt1*$^{+/+}$ (n=3) and *Sirt1*$^{Y/Y}$ (n=3) mice after 12 wk of normal chow or HFD (n=5/genotype) were measured after 20 h food withdrawal. Data are means ± SE. Unpaired t tests were performed to assess statistical significance. *$P < 0.05$, **$P < 0.005$, ***$P < 0.001$.

mice remained smaller. The calorie intake of the $Sirt1^{Y/Y}$ and $Sirt1^{+/+}$ mice was similar during HFD consumption (Fig. 1*D*).

Total body fat content was assessed by MRI imaging (23, 24). While fed the normal chow diet, the $Sirt1^{Y/Y}$ mice (**Fig. 2*A***) had a lower total body fat percentage and less visceral adiposity than did the $Sirt1^{+/+}$ mice (Fig. 2*C*). The fat content of both the $Sirt1^{Y/Y}$ and the $Sirt1^{+/+}$ mice increased significantly after 12 wk of HFD feeding (Fig. 2*A*, *B*) and there was no difference between the 2 strains (Fig. 2*C*).

The epididymal WAT pads from the $Sirt1^{Y/Y}$ mice fed the normal chow diet weighed less than those from the $Sirt1^{+/+}$ mice (Fig. 2*D*). After 12 wk of HFD, the WAT pads were similar in size for the 2 genotypes. Histologic sections of this WAT showed that adipocytes in the $Sirt1^{Y/Y}$ mice fed normal chow were smaller than those of the $Sirt1^{+/+}$ animals, that lipid droplets were enlarged in the HFD samples, and that the adipocytes from the $Sirt1^{Y/Y}$ HFD-fed animals were larger than those from the $Sirt1^{+/+}$ mice (Fig. 2*E*).

Adipocytes secrete leptin (25), and the leptin concentration in serum normally correlates with total body fat. Leptin concentrations in serum from $Sirt1^{Y/Y}$ mice fed normal chow diet were lower than those of their $Sirt1^{+/+}$ littermates (Fig. 2*F*). Leptin concentrations in the $Sirt1^{Y/Y}$ mice rose 27-fold after 12 wk of HFD feeding, whereas, in the $Sirt1^{+/+}$ mice, the concentration increased by a more modest 3-fold (Fig. 2*F*).

Histologic assessment of WAT from HFD-treated $Sirt1^{Y/Y}$ mice at 12 wk revealed no inflammation. However, WAT from $Sirt1^{Y/Y}$ mice maintained on the HFD for 23 wk showed extensive infiltration of lymphoid cells (Fig. 2*E*). Thus, the lymphoid cell infiltration of adipose tissue, often characteristic of animals fed the HFD, appeared to be a late event and was more severe in the $Sirt1^{Y/Y}$ than in the $Sirt1^{+/+}$ mice.

The interscapular BAT fat pads from the $Sirt1^{Y/Y}$ mice fed a normal chow diet were significantly smaller than those from the $Sirt1^{+/+}$ mice (**Fig. 3*A***). Following 12 wk of HFD, the BAT from the $Sirt1^{Y/Y}$ mice increased in size by 6.5-fold, a far more dramatic increase than seen in the $Sirt1^{+/+}$ mice. BAT adipocytes from animals on normal chow had multilocular lipid vacuoles, but the adipocytes from the $Sirt1^{Y/Y}$ mice fed the HFD became markedly enlarged, and many contained a prominent unilocular lipid droplet (Fig. 3*B*).

BAT adipocytes from the $Sirt1^{Y/Y}$ mice fed the HFD resembled adipocytes of WAT. The normal physiological function of BAT is thermogenesis, which is regulated by β-adrenergic receptors (26). To determine whether this function is compromised in BAT from $Sirt1^{Y/Y}$ mice, we injected animals with the selective β3-agonist CL-316243 and used indirect calorimetry to measure whole-animal respiration. The drug increased the Vo_2 rate and decreased the RER to similar extents in both the $Sirt1^{Y/Y}$ and the $Sirt1^{+/+}$ mice (Fig. 3*C*, *D*), indicating normal BAT function in the $Sirt1^{Y/Y}$ mice. Uncoupling protein 1 (UCP1) is a characteristic protein of BAT. UCP1 was detected by Western blots of protein from BAT of both the $Sirt1^{Y/Y}$ and the $Sirt1^{+/+}$ mice. No change was evident in UCP1 levels in BAT

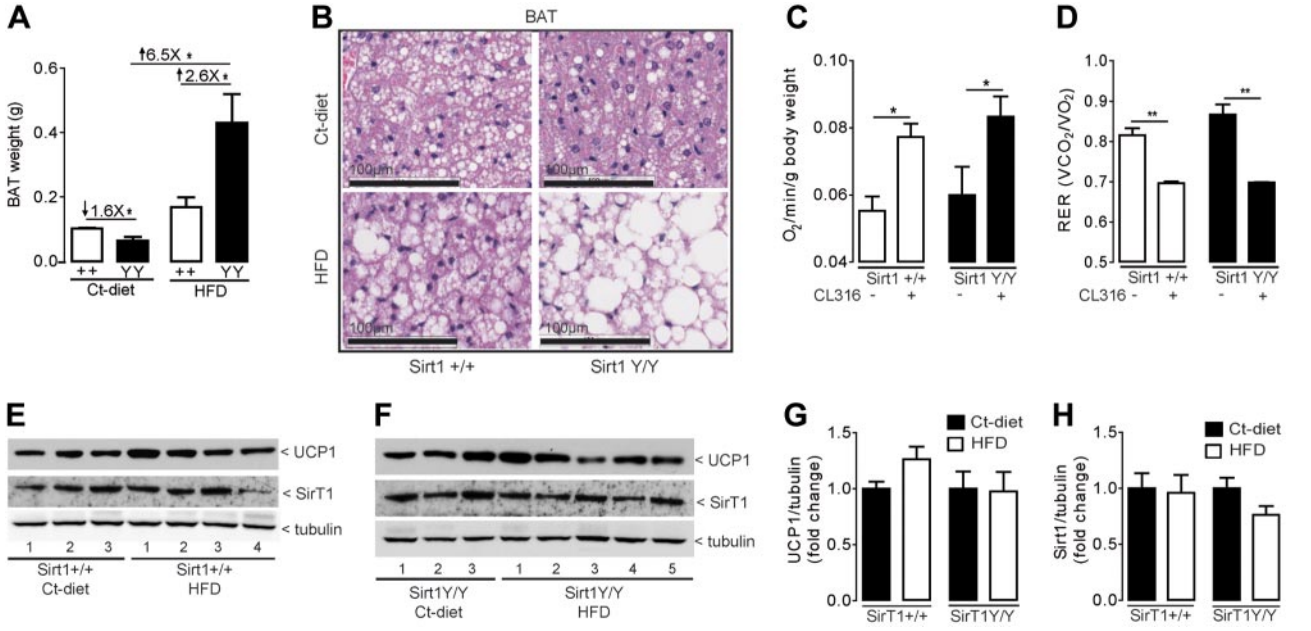

Figure 3. $Sirt1^{Y/Y}$ mice accumulate fat in BAT. *A*) Weights of interscapular BAT were obtained from 5- to 6-mo-old $Sirt1^{+/+}$ and $Sirt1^{Y/Y}$ mice fed normal chow (n=3/genotype) or an HFD for 12 wk (n=9–10/genotype). *B*) Histologic sections of BAT from $Sirt1^{Y/Y}$ mice fed HFD showed uncharacteristically enlarged adipocytes, many containing large, unilocular fat droplets. To assess BAT function, we used whole-animal, indirect calorimetry to measure Vo_2 and Vco_2 simultaneously. *C*, *D*) Whole-body O_2 normalized to body weight (ml/min/g; *C*) and RER (Vo_2/Vco_2; *D*) in mice injected with the β3-agonist CL-316243 (n=4/group). Data were averaged over 2 h after drug injection. *E*, *F*) Immunoblot detection of SIRT1, UCP1, and α-tubulin from BAT extracts from individual $Sirt1^{+/+}$ (*E*) and $Sirt1^{Y/Y}$ (*F*) mice. *G*, *H*) Densitometry of Western blot signals from *E* and *F*. Data are means ± SE. Unpaired t tests were performed to assess statistical significance. *$P < 0.05$, **$P < 0.005$, ***$P < 0.001$.

from mice fed an HFD (Fig. 3*E–H*). Thus, the adipocytes in the BAT from the HFD-fed *Sirt1*$^{Y/Y}$ mice accumulated lipid, but were not transformed into WAT.

Liver pathology in *Sirt1*$^{Y/Y}$ mice fed an HFD

The livers of the *Sirt1*$^{Y/Y}$ mice fed normal chow were 40% smaller than those of the *Sirt1*$^{+/+}$ animals, but increased in weight by 2.6-fold after 12 wk on an HFD (**Fig. 4*A***). The *Sirt1*$^{Y/Y}$ HFD livers were paler than those from the *Sirt1*$^{+/+}$ animals (Fig. 4*B*). Liver sections from the *Sirt1*$^{Y/Y}$ animals after 12 wk of HFD feeding indicated severe microvesicular steatosis. Hepatocytes were swollen, many with vacuoles (Fig. 4*E*) and lipid droplets (Fig. 4*F*). Although less severe, the liver pathology in the *Sirt1*$^{Y/Y}$ mice was evident after only 2 wk of the HFD (Fig. 4*C, D*).

The triglyceride content of livers from the *Sirt1*$^{Y/Y}$ animals increased significantly after only 2 wk of HFD consumption (Fig. 4*G*). The *Sirt1*$^{+/+}$ mice accumulated much less lipid and sustained much less obvious pathologic damage during the HFD challenge.

We used quantitative RT-PCR to compare the *Sirt1*$^{Y/Y}$ and *Sirt1*$^{+/+}$ livers for levels of transcripts encoding proteins involved in lipid metabolism: ABCA1, a cholesterol efflux transporter, and SREBP1, the master regulator of fat synthesis and the microsomal cytochrome p450 enzyme involved in the ω-oxidation of fatty acids (CyP4A14), a target gene of PPARα. No significant differences were found between the *Sirt1*$^{Y/Y}$ and *Sirt1*$^{+/+}$ mice, either before or after 12 wk of the HFD diet (data not shown). Both mouse strains also contained similar levels of interleukin-6 mRNA after 12 wk of the HFD (data not shown).

In contrast, the levels of SIRT1 protein detected by Western blot analysis were significantly increased in liver extracts prepared from the HFD-fed *Sirt1*$^{Y/Y}$ and *Sirt1*$^{+/+}$ mice (**Fig. 5*A–C***). This 2.5-fold increase in SIRT1 protein level was not accompanied by a change in the level of SIRT1 transcript (Fig. 5*D*), suggesting that the increase in SIRT1 and SIRT1(H355Y) proteins occurred at the post-transcription level, perhaps by elevated rates of translation or increased protein stability.

Immunohistochemical staining of liver sections (Fig. 5*E, F*) indicated that the SIRT1 and SIRT1(H355Y) proteins are largely (if not exclusively) nuclear, that staining was detected in hepatocytes, and that the intensity of staining increased in hepatocytes from both the *Sirt1*$^{Y/Y}$ and the *Sirt1*$^{+/+}$ mice after 12 wk of HFD feeding. No HFD-induced changes in SIRT1 levels were detected in the BAT (Fig. 3*E, F, H*).

Glucose homeostasis and bioenergetics in the *Sirt1*$^{Y/Y}$ mice

Oral glucose tolerance tests (OGTTs) were performed to assess the effect of the HFD diet on glucose homeostasis. In animals fed normal chow, the rise in blood glucose was consistently lower in the *Sirt1*$^{Y/Y}$ mice than in their *Sirt1*$^{+/+}$ littermates (**Fig. 6*A*, *B***). After 4 and 12 wk on HFD, the capacity of *Sirt1*$^{Y/Y}$ mice to handle the

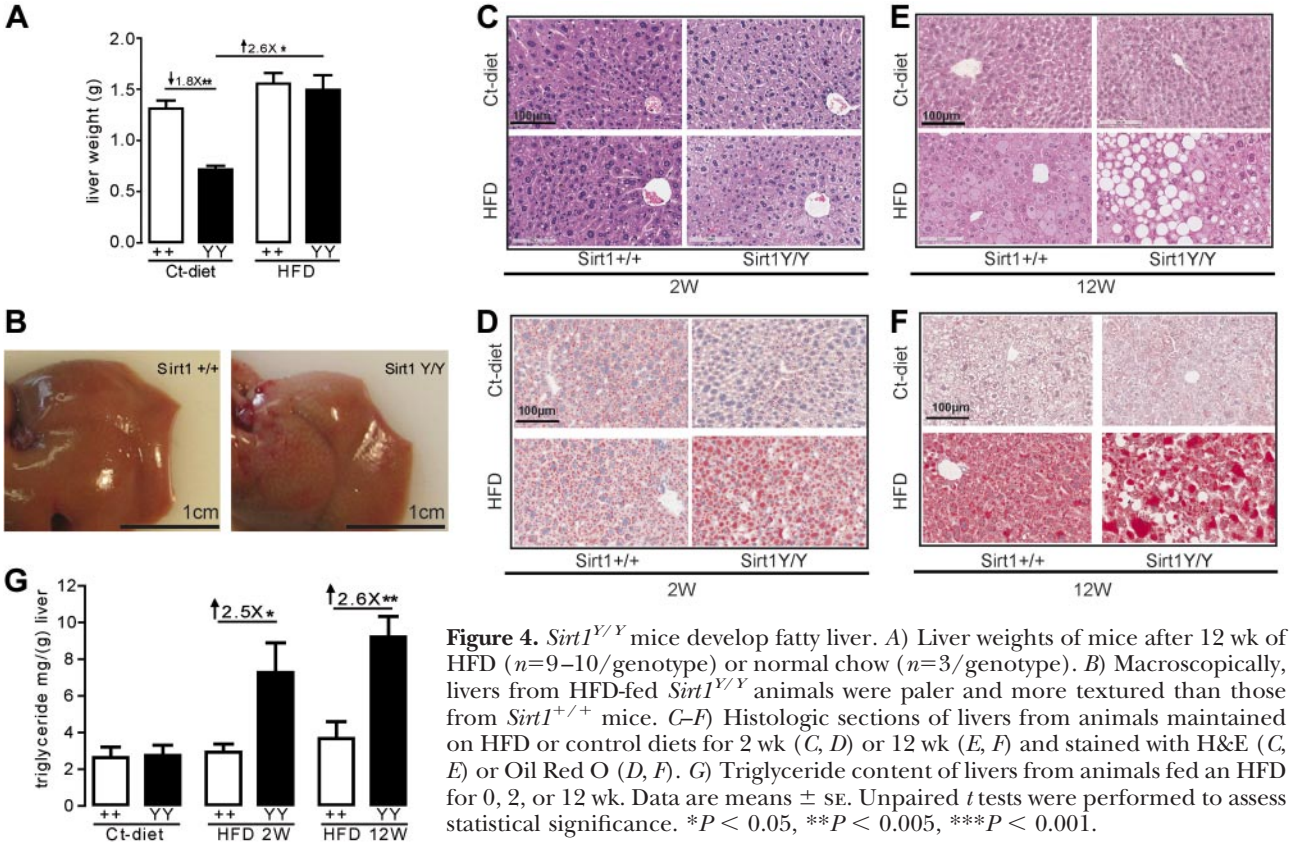

Figure 4. *Sirt1*$^{Y/Y}$ mice develop fatty liver. *A*) Liver weights of mice after 12 wk of HFD (n=9–10/genotype) or normal chow (n=3/genotype). *B*) Macroscopically, livers from HFD-fed *Sirt1*$^{Y/Y}$ animals were paler and more textured than those from *Sirt1*$^{+/+}$ mice. *C–F*) Histologic sections of livers from animals maintained on HFD or control diets for 2 wk (*C, D*) or 12 wk (*E, F*) and stained with H&E (*C, E*) or Oil Red O (*D, F*). *G*) Triglyceride content of livers from animals fed an HFD for 0, 2, or 12 wk. Data are means ± SE. Unpaired t tests were performed to assess statistical significance. *$P < 0.05$, **$P < 0.005$, ***$P < 0.001$.

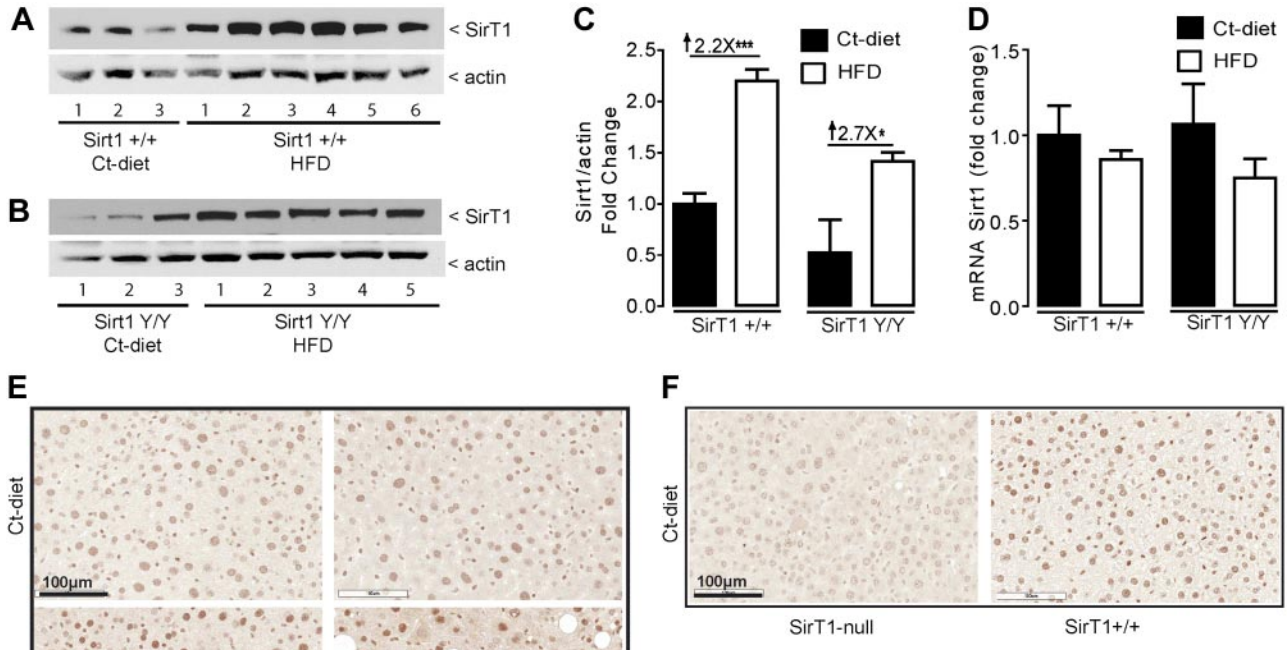

Figure 5. An HFD increases SIRT1 abundance in the liver. *A*, *B*) Immunoblots probed for SIRT1 and β-actin from liver extracts from $Sirt1^{+/+}$ (*A*) and $Sirt1^{Y/Y}$ (*B*) mice after 12 wk of HFD or normal chow. Each lane was run with an extract from a different mouse. *C*) Quantification of the Western blots from *A* and *B*. *D*) Relative amounts of *Sirt1* mRNA were measured by RT-qPCR from liver isolated from the same mice whose protein was assessed in *A*. *E*) Immunohistochemical staining of SIRT1 in liver sections. Positive staining for SIRT1 was found exclusively in the nuclei of hepatocytes. A stronger signal was evident in the livers of HFD-fed $Sirt1^{+/+}$ and $Sirt1^{Y/Y}$ mice. *F*) The livers of $Sirt1^{-/-}$ mice were used as a control for antibody specificity, because these animals have no detectable SIRT1 protein. Data are means ± SE. Unpaired *t* tests were performed to assess statistical significance. $*P < 0.05$, $**P < 0.005$, $***P < 0.001$.

bolus of glucose was significantly compromised. The effect of an HFD on glucose handling in the $Sirt1^{+/+}$ mice was much less profound. Area under the curve (AUC) values showed impaired glucose tolerance in the HFD-fed $Sirt1^{Y/Y}$ mice but a less dramatic effect on the HFD-fed $Sirt1^{+/+}$ mice (Fig. 6*C*).

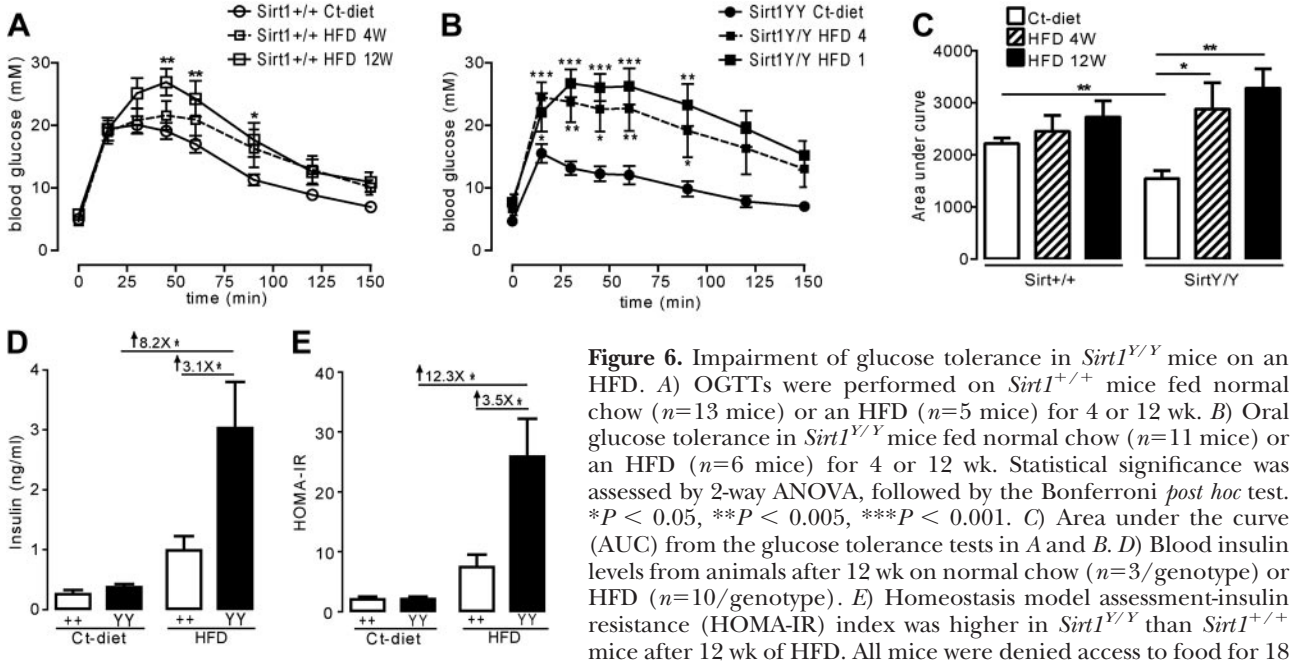

Figure 6. Impairment of glucose tolerance in $Sirt1^{Y/Y}$ mice on an HFD. *A*) OGTTs were performed on $Sirt1^{+/+}$ mice fed normal chow (n=13 mice) or an HFD (n=5 mice) for 4 or 12 wk. *B*) Oral glucose tolerance in $Sirt1^{Y/Y}$ mice fed normal chow (n=11 mice) or an HFD (n=6 mice) for 4 or 12 wk. Statistical significance was assessed by 2-way ANOVA, followed by the Bonferroni *post hoc* test. $*P < 0.05$, $**P < 0.005$, $***P < 0.001$. *C*) Area under the curve (AUC) from the glucose tolerance tests in *A* and *B*. *D*) Blood insulin levels from animals after 12 wk on normal chow (n=3/genotype) or HFD (n=10/genotype). *E*) Homeostasis model assessment-insulin resistance (HOMA-IR) index was higher in $Sirt1^{Y/Y}$ than $Sirt1^{+/+}$ mice after 12 wk of HFD. All mice were denied access to food for 18 h before blood sampling and before OGTTs. Data are means ± SE. Unpaired *t* tests were performed to assess statistical significance. $*P < 0.05$, $**P < 0.005$.

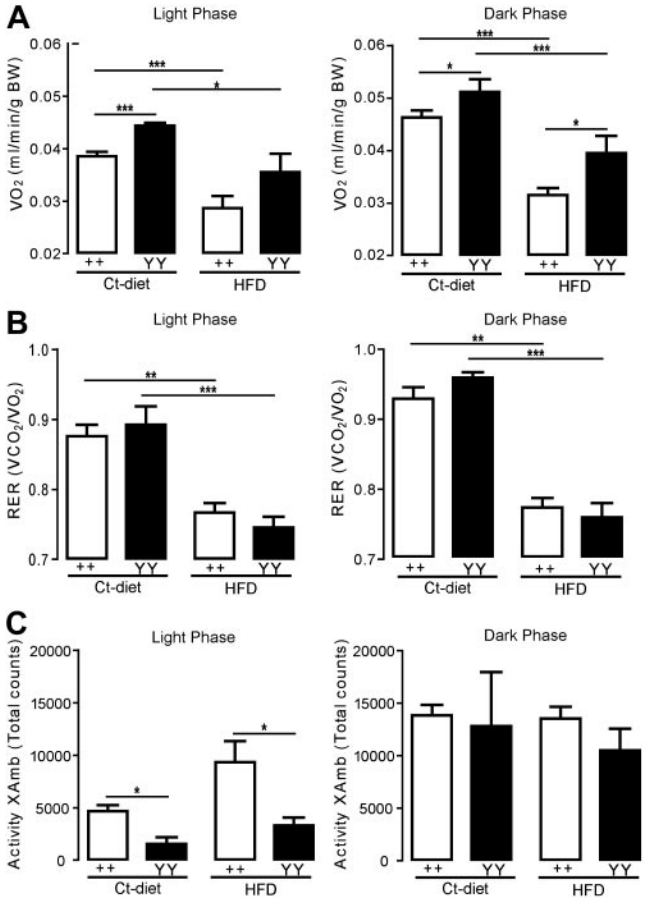

Figure 7. *Sirt1*$^{Y/Y}$ mice are hypermetabolic. Whole-animal indirect calorimetry was used to simultaneously measure Vo_2, RER (Vo_2/Vco_2), and horizontal ambulatory locomotor activity (X_{Amb}) over 24 h. *A*) Whole-body Vo_2 of *Sirt1*$^{Y/Y}$ mice was higher than that of *Sirt1*$^{+/+}$ littermates during the light and dark phases, regardless of the diet. Data were averaged separately over the light and the dark phases of the day (lights on 06:00–18:00). HFD decreased energy expenditure in both genotypes, but oxygen consumption of *Sirt1*$^{Y/Y}$ mice remained higher than that of *Sirt1*$^{+/+}$. *B*) RER decreased after 12 wk of HFD, reflecting an energy source switch toward lipid utilization, but the genotype had no effect on RER. *C*) *Sirt1*$^{Y/Y}$ mice were less active than *Sirt1*$^{+/+}$ animals during the light phase of the day (n=4–9/group). Data are means ± SE. Unpaired t tests were performed to assess statistical significance. $^*P < 0.05$, $^{**}P < 0.005$, $^{***}P < 0.001$.

The OGTT results suggested that the HFD-fed *Sirt1*$^{Y/Y}$ mice developed insulin resistance. Fasting insulin levels (Fig. 6*D*) were consistent with this expectation, with insulin levels in the *Sirt1*$^{Y/Y}$ mice increasing 8-fold after 12 wk on the HFD. The increase in insulin level in the HFD-fed *Sirt1*$^{+/+}$ mice was much lower. The homeostasis model-assessment of insulin resistance index (HOMA-IR) for *Sirt1*$^{Y/Y}$ mice (Fig. 6*E*) indicates that SIRT1 activity is an asset for maintaining insulin sensitivity in animals challenged with an HFD.

The Vo_2 rates by the *Sirt1*$^{Y/Y}$ mice were higher than those of the *Sirt1*$^{+/+}$ mice, in animals fed normal chow and those fed the HFD (**Fig. 7*A***). This elevated rate of respiration was evident in both the active and inactive circadian phases. The RER is an indirect measure of fuel type feeding the electron transport chain. The RERs of the *Sirt1*$^{Y/Y}$ and *Sirt1*$^{+/+}$ animals fed normal chow indicate that carbohydrates are the primary fuel, but the RER was significantly lower in HFD-fed mice of both genotypes (Fig. 7*B*), consistent with a shift toward fatty acid oxidation.

The spontaneous ambulatory activity of the *Sirt1*$^{Y/Y}$ and *Sirt1*$^{+/+}$ mice was similar during the active (dark) circadian phase, but the *Sirt1*$^{Y/Y}$ mice were much less active than the *Sirt1*$^{+/+}$ mice during the inactive (light) circadian phase (Fig. 7*C*). Thus, the elevated rate of respiration of *Sirt1*$^{Y/Y}$ mice (Fig. 7*A*) is not a consequence of increased activity.

Gut microbiota

Changes in the gut microbiota are related to obesity (27) and the development of fatty liver disease (28). We examined the gut microbiota in separately caged *Sirt1*$^{Y/Y}$ and *Sirt1*$^{+/+}$ mice fed normal chow and an HFD. The rDNA from fresh fecal samples were analyzed by a pyrosequencing approach (20). The microbial richness revealed by the Chao1 estimator was similar between the 2 genotypes, whatever the diet. The samples from normal chow were very similar, with only a few minor phyla and genera being differentially abundant, such as Fusobacteria and *Prevotella* (**Fig. 8*A*, *B***).

Firmicutes and Bacteroidetes were the dominant phyla in both mouse strains fed normal chow. After HFD feeding, the relative proportion of Firmicutes increased (Fig. 8*C*), whereas that of Bacteroidetes decreased (Fig. 8*D*), a result consistent with those in previous reports (1, 2). The rate at which this shift in abundance occurred was faster in the *Sirt1*$^{Y/Y}$ mice; significant changes were noted after only 1 wk of the HFD in the samples from the *Sirt1*$^{Y/Y}$ strain.

Ruminococcaceae (Fig. 8*E*) and *Alistipes* (Fig. 8*F*) are a family and a genus of the Firmicutes and the Bacteroidetes phyla, respectively, that show the same trends as the phyla. The HFD was associated with an increase in the genus *Enterococcus* only in the *Sirt1*$^{Y/Y}$ mice (Fig. 8*G*), whereas the Verrucomicrobia phylum (including the *Akkermansia* genus, Fig. 8*H*) disappeared completely in the *Sirt1*$^{Y/Y}$ mice after only 1 wk of an HFD.

DISCUSSION

After HFD challenge, mice lacking catalytically active SIRT1 developed rapid and severe characteristics of metabolic syndrome. These included liver steatosis, hypertrophy of both WAT and BAT, and insulin resistance. These physiological abnormalities were accompanied by changes in the gut microbiota. The more moderate response of mice expressing normal SIRT1 suggests that this enzyme plays a role in facilitating the organisms' adaptation to calorie overload. This conclusion is consistent with the more general inference that

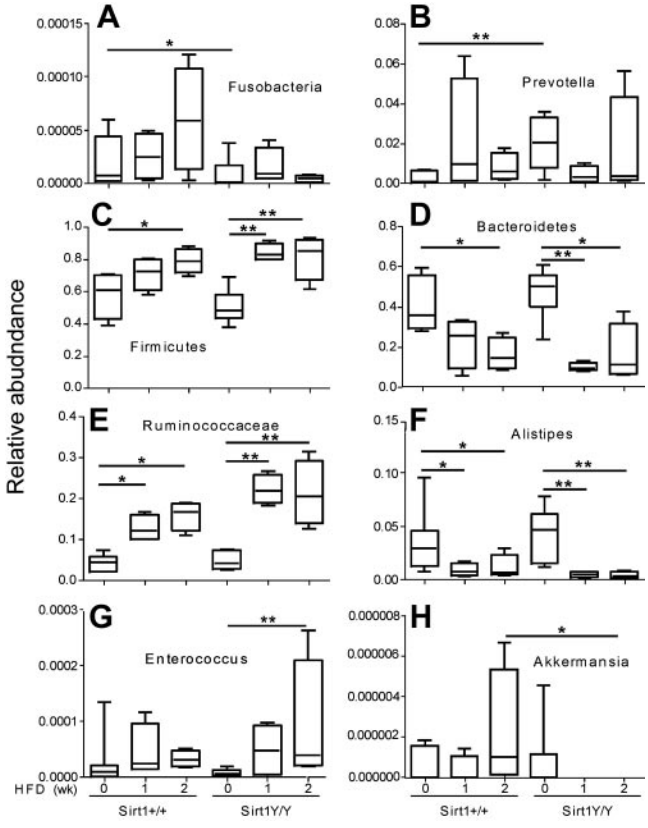

Figure 8. Gut microbiome response to an HFD. DNA was isolated from fresh fecal samples of $Sirt1^{Y/Y}$ and $Sirt1^{+/+}$ mice fed normal chow (0 wk of HFD; n=9, 7) or an HFD for 1 or 2 wk (n=4). The rDNA genes were sequenced, and the sequences were classified (20). *A*, *B*) A minor phylum (Fusobacteria; *A*) and genus (*Prevotella*; *B*) with differing abundance between the $Sirt1^{Y/Y}$ and $Sirt1^{+/+}$ mice fed normal chow. *C*, *D*) The major phyla Firmicutes (*C*) and Bacteroidetes (*D*), whose relative abundance changed after the switch to the HFD. *E*, *F*) The family Ruminococcaceae from the Firmicutes phylum (*E*) and the genus *Alistipes* from the Bacteroidetes phylum (*F*). *G*, *H*) The genera *Enterococcus* (*G*) and *Akkermansia* (*H*). Data are means ± SE. Two-tailed t tests were performed to assess statistical significance. $^*P < 0.05$, $^{**}P < 0.005$.

the role of the *Sirt1* gene is to accelerate acclimation to chronic stress (7).

Both $Sirt1^{-/-}$ and $Sirt1^{Y/Y}$ mice are smaller than $Sirt1^{+/+}$ animals, but consume as many calories and as much oxygen as their larger wild-type littermates (15, 17). This hypermetabolic state persists in the face of HFD feeding, but despite the excess rate of calorie disposal, the $Sirt1^{Y/Y}$ mice are less able than the $Sirt1^{+/+}$ animals to avoid developing the pathologies associated with metabolic syndrome. Previous reports have indicated that liver-specific knockout of the SIRT1 protein results in hepatic lipid accumulation (12, 29) and, conversely, that elevated SIRT1 is protective (11, 30). The elevated levels of SIRT1 protein found in livers of both the $Sirt1^{+/+}$ and $Sirt1^{Y/Y}$ mice after prolonged (12 wk) HFD feeding are consistent with the idea that SIRT1 plays a role in adaptation to the HFD challenge. It is interesting that this elevation in protein level took place in the absence of change in SIRT1 mRNA abundance. The increased SIRT1 protein may be a consequence of changes in mRNA translation, a level of regulation that may be mediated by the many miRNAs that have been shown to bind the 3′UTR of the SIRT1 mRNA (31).

The means by which SIRT1 effects its health benefits are elusive. Among the many documented substrates of SIRT1 are PGC-1α (9), PPARγ (8), and LXR (13). Each of these transcription factors or cofactors is thought to regulate the expression of genes whose products are responsible for mitochondrial genesis and lipid metabolism. However, discrepancies have become apparent when comparing studies that rely on cell culture systems with those *in vivo* (32), casting doubt on the relevance of many of the documented associations between SIRT1 and its substrates. Our attempts to identify SIRT1 targets have similarly resulted in failure to confirm previous inferences from the literature. For example, deacetylation of PCG-1α by SIRT1 has been reported to be necessary for the shift from glucose to lipid oxidation (33), but we found that $Sirt1^{Y/Y}$ mice readily underwent this shift when feeding was changed from carbohydrate-rich chow to an HFD. SIRT1 is reported to deacetylate and activate LXR to enhance transcription of ABCA1 (13), but we found similar levels of ABCA1 mRNA in the $Sirt1^{+/+}$ and $Sirt1^{Y/Y}$ mice.

The development of a fatty liver is modulated by nutrition, host genetics (2), and gut microbes (34). We found that the *Sirt1* genotype had very little effect on the distribution of bacteria in the gut of animals maintained on normal chow, but the change to an HFD resulted in a rapid shift in the prevalence of the major phyla. Of interest, the increased ratio of Firmicutes and Bacteroidetes occurred more rapidly in the $Sirt1^{Y/Y}$ animals, consistent with the general observation that the SIRT1 enzyme is involved in buffering the organism against chronic perturbation. The *Akkermansia* genus disappeared completely from the $Sirt1^{Y/Y}$ mice after only 1 wk of HFD, a result consistent with a recent report showing decreased *Akkermansia* in obese and type 2 diabetic mice (35). The relationship between gut microbiota and fatty liver has been noted (28, 34, 36) but the cause–effect relationships remain enigmatic. The gut microbiota may enhance adiposity by increasing the extraction of calories from food (34, 37), and SIRT1 activity may modify the intestinal niche(s) in which microbes grow by influencing the synthesis and secretion of host-derived antimicrobial peptides or by modulating the efficiency with which nutrients are absorbed by the gut.

SIRT1 has >80 documented substrates (7) and a much larger number of proteins with which it interacts (38). Experimental studies have reported a remarkably varied spectrum of cellular and physiological processes that are apparently regulated by SIRT1 (39). Yet mice born with either no SIRT1 protein (16) or with the catalytically inactive SIRT1(H355Y) protein (17) are viable and have few

of the expected physiological deficits. One interpretation of this paradox is that SIRT1 is a hub in a complex, scale-free network of proteins (7). Many of SIRT1's neighbors in this network are themselves subject to regulation and mutation (particularly in cell cultures), so that the nature of the network and the role of SIRT1 in this network are dynamic. Our study and many others performed in animals carrying genetically altered expression of SIRT1 suggest that the main function of SIRT1 is to mediate adaptation of chronic stresses. How the SIRT1 scale-free network accomplishes this buffering against various perturbations is not yet clear, but it most likely involves multiple substrates and feedback systems that are inherent characteristics of networks (7). FJ

The authors thank Dr. Manijeh Daneshmand for help with analysis of the histology. This work was supported by grants from the Canadian Institutes for Health Research.

REFERENCES

1. Turnbaugh, P. J., Backhed, F., Fulton, L., and Gordon, J. I. (2008) Diet-induced obesity is linked to marked but reversible alterations in the mouse distal gut microbiome. *Cell Host Microbe* **3,** 213–223
2. Parks, B. W., Nam, E., Org, E., Kostem, E., Norheim, F., Hui, S. T., Pan, C., Civelek, M., Rau, C. D., Bennett, B. J., Mehrabian, M., Ursell, L. K., He, A., Castellani, L. W., Zinker, B., Kirby, M., Drake, T. A., Drevon, C. A., Knight, R., Gargalovic, P., Kirchgessner, T., Eskin, E., and Lusis, A. J. (2013) Genetic control of obesity and gut microbiota composition in response to high-fat, high-sucrose diet in mice. *Cell Metab.* **17,** 141–152
3. Imai, S., Armstrong, C. M., Kaeberlein, M., and Guarente, L. (2000) Transcriptional silencing and longevity protein Sir2 is an NAD-dependent histone deacetylase. *Nature* **403,** 795–800
4. Smith, J. S., Brachmann, C. B., Celic, I., Kenna, M. A., Muhammad, S., Starai, V. J., Avalos, J. L., Escalante-Semerena, J. C., Grubmeyer, C., Wolberger, C., and Boeke, J. D. (2000) A phylogenetically conserved NAD+-dependent protein deacetylase activity in the Sir2 protein family. *Proc. Natl. Acad. Sci. U. S. A.* **97,** 6658–6663
5. Landry, J., Sutton, A., Tafrov, S. T., Heller, R. C., Stebbins, J., Pillus, L., and Sternglanz, R. (2000) The silencing protein SIR2 and its homologs are NAD-dependent protein deacetylases. *Proc. Natl. Acad. Sci. U. S. A.* **97,** 5807–5811
6. Lemieux, M. E., Yang, X., Jardine, K., He, X., Jacobsen, K. X., Staines, W. A., Harper, M. E., and McBurney, M. W. (2005) The Sirt1 deacetylase modulates the insulin-like growth factor signaling pathway in mammals. *Mech. Ageing Dev.* **126,** 1097–1105
7. McBurney, M. W., Clark-Knowles, K. V., Caron, A. Z., and Gray, D. A. (2013) SIRT1 Is a highly networked protein that mediates the adaptation to chronic physiological stress. *Genes Cancer* **4,** 125–134
8. Picard, F., Kurtev, M., Chung, N., Topark-Ngarm, A., Senawong, T., Oliveira, R. M., Leid, M., McBurney, M. W., and Guarente, L. (2004) Sirt1 promotes fat mobilization in white adipocytes by repressing PPAR-gamma. *Nature* **429,** 771–776
9. Rodgers, J. T., Lerin, C., Haas, W., Gygi, S. P., Spiegelman, B. M., and Puigserver, P. (2005) Nutrient control of glucose homeostasis through a complex of PGC-1α and SIRT1. *Nature* **434,** 113–118
10. Motta, M. C., Divecha, N., Lemieux, M., Kamel, C., Chen, D., Gu, W., Bultsma, Y., McBurney, M., and Guarente, L. (2004) Mammalian SIRT1 represses forkhead transcription factors. *Cell* **116,** 551–563
11. Pfluger, P. T., Herranz, D., Velasco-Miguel, S., Serrano, M., and Tschop, M. H. (2008) Sirt1 protects against high-fat diet-induced metabolic damage. *Proc. Natl. Acad. Sci. U. S. A.* **105,** 9793–9798
12. Purushotham, A., Schug, T. T., Xu, Q., Surapureddi, S., Guo, X., and Li, X. (2009) Hepatocyte-specific deletion of SIRT1 alters fatty acid metabolism and results in hepatic steatosis and inflammation. *Cell Metab.* **9,** 327–338
13. Li, X., Zhang, S., Blander, G., Tse, J. G., Krieger, M., and Guarente, L. (2007) SIRT1 deacetylates and positively regulates the nuclear receptor LXR. *Mol. Cell* **28,** 91–106
14. Purushotham, A., Xu, Q., Lu, J., Foley, J. F., Yan, X., Kim, D. H., Kemper, J. K., and Li, X. (2012) Hepatic deletion of SIRT1 decreases HNF1alpha/FXR signaling and induces formation of cholesterol gallstones in mice. *Mol. Cell. Biol.* **32,** 1226–1236
15. Boily, G., Seifert, E. L., Bevilacqua, L., He, X. H., Sabourin, G., Estey, C., Moffat, C., Crawford, S., Saliba, S., Jardine, K., Xuan, J., Evans, M., Harper, M. E., and McBurney, M. W. (2008) SirT1 regulates energy metabolism and response to caloric restriction in mice. *PLoS ONE* **3,** e1759
16. McBurney, M. W., Yang, X., Jardine, K., Hixon, M., Boekelheide, K., Webb, J. R., Lansdorp, P. M., and Lemieux, M. (2003) The mammalian SIR2alpha protein has a role in embryogenesis and gametogenesis. *Mol. Cell. Biol.* **23,** 38–54
17. Seifert, E. L., Caron, A. Z., Morin, K., Coulombe, J., Hong, H., X, Jardine, K., Dewar-Darch, D., Boekelheide, K., Harper, M. E., and McBurney, M. W. (2012) SirT1 catalytic activity is required for male fertility and metabolic homeostasis in mice. *FASEB J.* **26,** 555–566
18. Salmon, D. M., and Flatt, J. P. (1985) Effect of dietary fat content on the incidence of obesity among ad libitum fed mice. *Int. J. Obes.* **9,** 443–449
19. Arthur, J. C., Perez-Chanona, E., Muhlbauer, M., Tomkovich, S., Uronis, J. M., Fan, T. J., Campbell, B. J., Abujamel, T., Dogan, B., Rogers, A. B., Rhodes, J. M., Stintzi, A., Simpson, K. W., Hansen, J. J., Keku, T. O., Fodor, A. A., and Jobin, C. (2012) Intestinal inflammation targets cancer-inducing activity of the microbiota. *Science* **6103,** 120–123
20. Sundquist, A., Bigdeli, S., Jalili, R., Druzin, M. L., Waller, S., Pullen, K. M., El-Sayed, Y. Y., Taslimi, M. M., Batzoglou, S., and Ronaghi, M. (2007) Bacterial flora-typing with targeted, chip-based pyrosequencing. *BMC Microbiol.* **7,** 108
21. Magoc, T., and Salzberg, S. L. (2011) FLASH: fast length adjustment of short reads to improve genome assemblies. *Bioinformatics* **27,** 2957–2963
22. Caporaso, J. G., Kuczynski, J., Stombaugh, J., Bittinger, K., Bushman, F. D., Costello, E. K., Fierer, N., Pena, A. G., Goodrich, J. K., Gordon, J. I., Huttley, G. A., Kelley, S. T., Knights, D., Koenig, J. E., Ley, R. E., Lozupone, C. A., McDonald, D., Muegge, B. D., Pirrung, M., Reeder, J., Sevinsky, J. R., Turnbaugh, P. J., Walters, W. A., Widmann, J., Yatsunenko, T., Zaneveld, J., and Knight, R. (2010) QIIME allows analysis of high-throughput community sequencing data. *Nat. Methods* **7,** 335–336
23. Ye, Q., Mei, Y., and Rudin, M. (2012) Novel strategy to differentiate water and lipid composition. *Proc. Intl. Soc. Mag. Reson. Med.* **20,** 1368
24. Cron, G. O., Mailloux, R. J., Harper, M. E., and Schweitzer, M. E. (2013) Whole-mouse MR imaging of fat fraction at 7 Tesla using a Fourier-based many-echo technique. *Proc. Intl. Soc. Mag. Reson. Med.* **21,** 1522
25. Masuzaki, H., Ogawa, Y., Isse, N., Satoh, N., Okazaki, T., Shigemoto, M., Mori, K., Tamura, N., Hosoda, K., and Yoshimasa, Y. (1995) Human obese gene expression: adipocyte-specific expression and regional differences in the adipose tissue. *Diabetes* **44,** 855–858
26. Cannon, B., and Nedergaard, J. (2004) Brown adipose tissue: function and physiological significance. *Physiol. Rev.* **84,** 277–359
27. Turnbaugh, P. J., Ley, R. E., Mahowald, M. A., Magrini, V., Mardis, E. R., and Gordon, J. I. (2006) An obesity-associated gut microbiome with increased capacity for energy harvest. *Nature* **444,** 1027–1031

28. Le, R. T., Llopis, M., Lepage, P., Bruneau, A., Rabot, S., Bevilacqua, C., Martin, P., Philippe, C., Walker, F., Bado, A., Perlemuter, G., Cassard-Doulcier, A. M., and Gerard, P. (2013) Intestinal microbiota determines development of non-alcoholic fatty liver disease in mice. *Gut* **62,** 1787–1794
29. Wang, R. H., Li, C., and Deng, C. X. (2010) Liver steatosis and increased ChREBP expression in mice carrying a liver specific SIRT1 null mutation under a normal feeding condition. *Int. J. Biol. Sci.* **6,** 682–690
30. Banks, A. S., Kon, N., Knight, C., Matsumoto, M., Gutiérrez-Juárez, R., Rossetti, L., Gu, W., and Accili, D. (2008) SirT1 gain of function increases energy efficiency and prevents diabetes in mice. *Cell Metab.* **8,** 333–341
31. Yamakuchi, M. (2012) MicroRNA Regulation of SIRT1. *Front. Physiol.* **3,** 68
32. Philp, A., and Schenk, S. (2013) Unraveling the complexities of SIRT1-mediated mitochondrial regulation in skeletal muscle. *Exerc. Sport Sci. Rev.* **41,** 174–181
33. Gerhart-Hines, Z., Rodgers, J. T., Bare, O., Lerin, C., Kim, S. H., Mostoslavsky, R., Alt, F. W., Wu, Z., and Puigserver, P. (2007) Metabolic control of muscle mitochondrial function and fatty acid oxidation through SIRT1/PGC-1alpha. *EMBO J.* **26,** 1913–1923
34. Backhed, F., Ding, H., Wang, T., Hooper, L. V., Koh, G. Y., Nagy, A., Semenkovich, C. F., and Gordon, J. I. (2004) The gut microbiota as an environmental factor that regulates fat storage. *Proc. Natl. Acad. Sci. U. S. A.* **101,** 15718–15723
35. Everard, A., Belzer, C., Geurts, L., Ouwerkerk, J. P., Druart, C., Bindels, L. B., Guiot, Y., Derrien, M., Muccioli, G. G., Delzenne, N. M., de Vos, W. M., and Cani, P. D. (2013) Cross-talk between *Akkermansia muciniphila* and intestinal epithelium controls diet-induced obesity. *Proc. Natl. Acad. Sci. U. S. A.* **110,** 9066–9071
36. Spencer, M. D., Hamp, T. J., Reid, R. W., Fischer, L. M., Zeisel, S. H., and Fodor, A. A. (2011) Association between composition of the human gastrointestinal microbiome and development of fatty liver with choline deficiency. *Gastroenterology* **140,** 976–986
37. Backhed, F., Manchester, J. K., Semenkovich, C. F., and Gordon, J. I. (2007) Mechanisms underlying the resistance to diet-induced obesity in germ-free mice. *Proc. Natl. Acad. Sci. U. S. A.* **104,** 979–984
38. Sharma, A., Gautam, V., Costantini, S., Paladino, A., and Colonna, G. (2012) Interactomic and pharmacological insights on human sirt-1. *Front. Pharmacol.* **3,** 40
39. Morris, B. J. (2012) Seven sirtuins for seven deadly diseases of aging. *Free Radic. Biol. Med.* **56,** 133–171

Received for publication October 3, 2013.
Accepted for publication November 18, 2013.